ADVANCED
ENERGY
MATERIALS

Supporting Information

for *Adv. Energy Mater.*, DOI 10.1002/aenm.202204411

In Situ Topological Interphases Boosting Stable Solid-State Lithium Metal Batteries

Hantao Xu, Jianyong Zhang, Hong Zhang, Juncai Long, Lin Xu and Liqiang Mai**

Supporting Information

In Situ Topological Interphases Boosting Stable Solid-State Lithium Metal Batteries

Hantao Xu, Jianyong Zhang, Hong Zhang, Juncai Long, Lin Xu,* Liqiang Mai.*

H. T. Xu, J. Y. Zhang, H. Zhang, J. C. Long, Prof. L. Xu, Prof. L. Q. Mai
State Key Laboratory of Advanced Technology for Materials Synthesis and Processing, School of Materials Science and Engineering, Wuhan University of Technology, Wuhan 430070, P.R. China.
E-mail: linxu@whut.edu.cn (Prof. L. Xu), mlq518@whut.edu.cn (Prof. L. Q. Mai)

Prof. L. Xu, Prof. L. Q. Mai
Hubei Longzhong Laboratory, Wuhan University of Technology (Xiangyang Demonstration Zone), Xiangyang 441000, Hubei, P.R. China.
Hainan Institute, Wuhan University of Technology, Sanya 572000, P.R. China.
E-mail: linxu@whut.edu.cn (Prof. L. Xu), mlq518@whut.edu.cn (Prof. L. Q. Mai)

Keywords: solid-state electrolytes, topological interphases, poly-dioxolane, solid electrolyte interfaces, lithium metal anodes

1. Experimental Details

1.1. Materials

Ethylene glycol, trimethylamine (TEA), 2-isocyanatoethylmethacrylate, AIBN (recrystallization), 1,3-dioxolane (DOL), Al(OTf)$_3$ and dimethyl sulfoxide-d$_6$ were purchased from Aladdin Co. Ltd. Bis(trifluoromethane) sulfonamide lithium (LiTFSI) was purchased from Sigma-Aldrich. Anhydrous ethanol, dichloromethane, dimethyl sulfoxide (DMSO), tetrahydrofuran (THF), N,N-dimethylformamide (DMF) and anhydrous ether were purchased from Sinopharm Chemical Reagent Co. Ltd. The above all the chemicals were used directly as purchased without further purification treatment.

1.2. Synthesis of poly(1,3-dioxolane) (PDOL)

5 g DOL and three drops of ethylene glycol were added to a 100 mL three-neck flask equipped with a magnetic stir bar and nitrogen purge. Then, 0.02 g Al(OTf)$_3$ was added into the mixture and stirred at room temperature overnight. After vacuum drying at room temperature for 6 hours, a white solid of hydroxyl-terminated PDOL was obtained. The ^{1}H NMR (400 MHz, DMSO-d$_6$) of PDOL can be seen in **Figure S29**.

1.3. Synthesis of poly(1,3-dioxolane) urethane dimethacrylate (PDOLUDMA)

1 g hydroxyl-terminated PDOL, one drop of triethylamine, 20 mL of anhydrous dichloromethane were added to a 100 mL three-neck flask equipped with a magnetic stir bar and nitrogen purge under an ice water bath. Then, 0.05 g 2-isocyanatoethylmethacrylate was added dropwise to the mixture at 0 ^{o}C and then stirred overnight at room temperature. After the reaction was quenched by deionized water, a white solid was precipitated in anhydrous ether from organic phase. After being washed with anhydrous ether, cold deionized water and cold THF for three times respectively, the white solid (1 g) was obtained. Then, the white solid was vacuum dried at 20 ^{o}C for 6 hours. The ^{1}H NMR (400 MHz, DMSO-d$_6$) of PDOLUDMA can be seen in **Figure 2**a.

1.4. Synthesis of cross-linked PDOL (CPDOL)

0.5 g PDOLUDMA and 5 ml DMF were added into a 20 mL vial with a magnetic stir bar after nitrogen purge. Then, 0.005 g AIBN was added into the mixture and stirred at 50 ^{o}C overnight. After the reaction was complete, a clear gel was obtained (**Figure S30**), and then, a white solid was precipitated in anhydrous ether from organic phase. After being washed with anhydrous ether and cold THF for three times, the product of white solid (0.5 g) was vacuum dried at 50 ^{o}C for 6 hours. The ^{1}H NMR (400 MHz, DMSO-d$_6$) of CPDOL can be seen in

Figure S31. In order to determine the chemical shift of the active hydrogen of −NH, proton exchange experiment with the addition of heavy water was carried out (**Figure S32**).

1.5. Preparation of CPDOL-SPE

0.5 g CPDOL was added in 40 mL anhydrous DMF and vigorously stirred until completely dissolved. In the meanwhile, 0.4 g LiTFSI was added and stirred by magnetic agitation and heated room temperature for 2 h. The resultant liquid-like solution was evenly casted on a 5 μm PE fibres on a Teflon plate by a doctor blade to form a uniform membrane. The as-prepared membrane was vacuum-dried at 80 °C for 12 h to remove the residue solvent and H_2O. The flexible and adhesive SPE was obtained. Then, the cathode foil was punched into small plates with a diameter of 17 mm. The water content of CPDOL-SPE measured by Karl Fischer titrator was 27.627 ppm.

1.6. Calculations

The electrostatic potential (ESP) and orbital composition analysis of the highest occupied molecular orbital/lowest unoccupied molecular orbital (HOMO/LUMO) were run on Gaussian 09 package and calculated on the basis of B3LYP/6-31+G*. The electrostatic potential (ESP) and orbital composition analysis of the highest occupied molecular orbital/lowest unoccupied molecular orbital (HOMO/LUMO) were derived from the optimized structure. The visualization of theoretical calculations was conducted by Gaussview.

The spin-polarized density functional theory (DFT) simulations were carried out with help of the Vienna ab initio Simulation Program (VASP).[1] The Projector Augmented Wavefunction (PAW) method was used to describe the inert core electrons. The Perdew-Burke-Ernzerhof (PBE) was employed for describing the electronic exchange-correlation interactions.[2] The kinetic energy cutoff for the plane-wave basis was set to 520 eV and the k-points was set to 1×1×1. The convergence criteria of structure optimization were chosen as the maximum force of 0.02 eV/Å, and the energy change of 1×10^{-5} eV/atom. The DFT-D3 method with Becke-Johnson (BJ) damping was employed to describe the van der Waals interactions.[3]

1.7. Materials characterization

The morphology of SPE membranes and the surface of SEIs on the lithium metal anodes w ere examined via a JEOL JSM-7100F scanning electron microscope with an accelerating voltage of 20 kV. After the battery is disassembled, the SPE membrane near the lithium metal side was measured with Fourier transform infrared spectrometer (FT-IR) using the reflection method. (Thermo Nicolet Corporation; 7800-350/cm 0.01/cm/6700). Nuclear magnetic resonance (NMR) (Bruker 400 MHz, DMSO−d_6) was used to analyze the structure of samples. The electrolyte after cycling was precipitated in diethyl ether for complete removal of lithium salts, followed by characterization of ^{7}Li NMR in DMSO-d_6. The X-ray photoelectron spectroscopy (XPS, ESCALAB 250 Xi spectrometer) analyses were used to measure the surface composition of the SPEs on the side near the lithium metal, and the surface composition and elements content of the SEIs on the surface of lithium metal and further composition information at different depths, while the preparations and samplings were protected in a glove box full of Ar inert gas. GPC was recorded by an Agilent 1200 series HPLC with an MZ-GPC column and DMF was used as the elution solvent with a flow rate of 1.0 mL min^{-1} and polystyrene was used as a standard. AFM (Asylum Research, MFP-3D) was used to measure the morphology, force curves and Young's modulus of the surface of interphase (the surface of lithium metal anode in contact with SPE), while the instrument was protected in a glove box full of Ar inert gas. The water content of CPDOL-SPE was measured by Karl Fischer titrator (Mettler Toledo C20S). MALDI-TOF-MS was recorded by a Bruker Ultraflextreme (355 nm Nd:YAG laser, 2000 Hz), and the sample was prepared by mixing a solution of matrix (CHCA) in DMF. Then, 1 μL of the resulting mixture was deposited onto the target plate and the solvent was evaporated. Solid-state ^{19}F NMR spectra of electrolyte membranes were measured in a double resonance 2.5 mm magic angle spinning probe on a Bruker Avance 500 spectrometer with a spinning frequency of 15 kHz and the 19 Li shifts were referenced to KF (125.3 ppm).

1.8. Electrochemical measurements

The activation energy for Li^+ transport through SEI was based on the temperature-dependent EIS measurement of Li/Li cell (20~70°C). The activation energy can be obtained according to the relation of $Ea = -19.144 \times \text{slope}$ (kJ mol^{-1}), where the slope can be obtained by impedance at different temperatures. Tafel plots were acquired from a CV test in Li/Li cells with a scan rate of 1.0 mV s$^{-1.}$ The selected voltage ranges from 80 to 100 mV in the linear region were employed to calculate exchange current density (i_0).

1.9. Ionic Conductivity and activation energy

The stainless steel SS/SPE/SS cells were assembled to measure ionic conductivities. 2mL CPDOL-SPE in DMF was deposited on a 15.8 mm stainless steel sheet, followed by vacuum drying at 80 °C for 6 h. The electrochemical impedance spectroscopy (EIS) was measured in the temperature range from 20 °C to 80 °C (record every 10 °C) using an Autolab PGSTAT302N in the frequency range from 10^6 Hz to 10^2 Hz with a perturbation of 10 mV.

The SPE was sandwiched between two pieces of stainless-steel blocking electrode with a diameter of 15.8 mm. and the ionic conductivity(σ)was calculated from the Equation (1):

$$\sigma = \frac{L}{R_b S} \qquad (1)$$

Where L is the thickness of the SPE, S is the contact area between the two stainless steel plates, and R(Ω) is the bulk resistance of the SPE.

1.10. Electrochemical Stability Window

The Electrochemical Stability Window of electrolytes can be measured by building Li/SPE/SS cells and conducting linear sweep voltammetry (LSV) measurements range from 0−6 V at 1 mV s^{-1} via Autolab PGSTAT302N.

1.11. Li^+ Transference Number

Li^+ Transference Number can be tested using Li/SPE/Li symmetric cells at 60 ^oC via Autolab PGSTAT302N. The cell resistances are determined before and after polarization using EIS and currents measured by the DC method. t_{Li}^+ is obtained according to the following Equation (2):

$$t_{Li+} = \frac{I_s(\Delta V - I_0 R_0)}{I_0(\Delta V - I_s R_s)} \qquad (2)$$

Where I_0 and I_s are the initial and steady-state currents. The R_0 and R_s are the resistances before and after polarization of the cell, respectively. ΔV is the DC potential applied across the cell.

1.12. Battery assembly and testing

Li/SPE/Li symmetric cells assembled in an argon-filled glovebox (H_2O < 0.01 ppm, O_2 < 0.01 ppm) were tested by a multichannel battery testing system (Land CT2001A, Wuhan Land Electronic Co. Ltd., China). A certain constant current density was applied to the battery and the current signal was changed every 60 minutes at 60 ^oC. The SEM images of the cycled lithium metal anodes were disassembled after 100 hours of cycling and washed with DME. The rate and cycle performance of SPE-based cells were performed by using $LiFePO_4$/SPE/Li (100 or 600 μm, 14 mm) coin cells assembled in an argon-filled glovebox. The $LiFePO_4$ cathode slurry was prepared by commercially available cathode powder, Super P, and PVDF powder with a mass fraction of 8:1:1. The obtained cathode slurry was doctor-bladed on aluminum foils and then dried at 120 °C for 12 h in a vacuum oven. Then, the cathode foil was punched into small plates with a diameter of 10 mm, which shows a mass loading of 0.8~1.8 mg cm^{-2}. The C rates in all of the electrochemical measurements are defined based on 1C = 170 mAh g^{-1}. The as-prepared CR2016 cells then subjected to test its charging/discharging cyclic performance and rate capability by charging to 4 V and discharging to 2.5 V at 60 ^{o}C on LAND testing system.

2. Supplementary figures

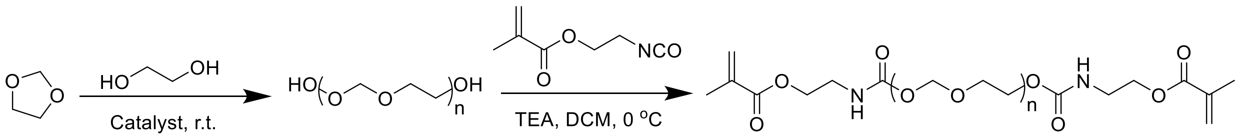

Figure S1. Synthetic route of PDOLUDMA.

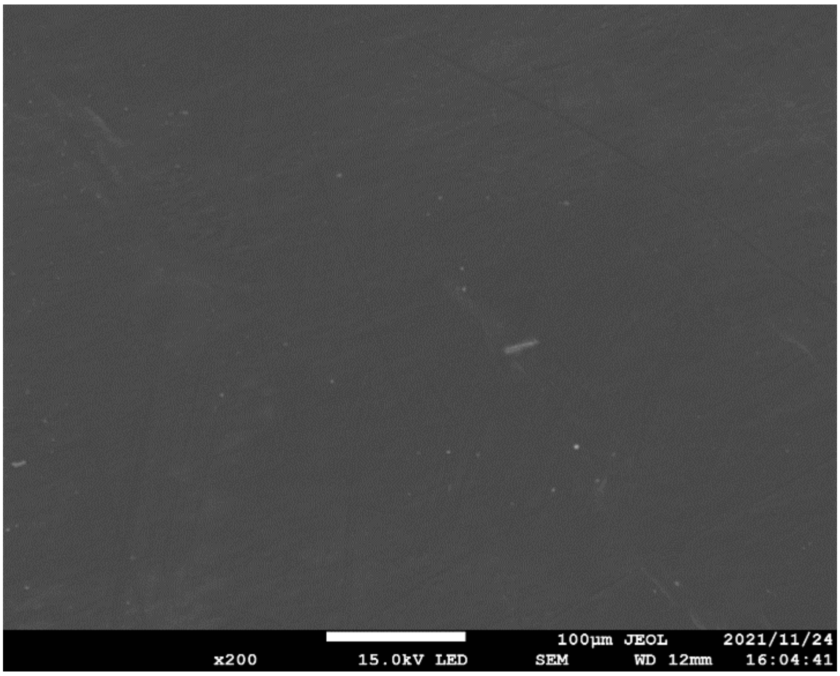

Figure S2. Top view of SEM image of CPDOL-SPE.

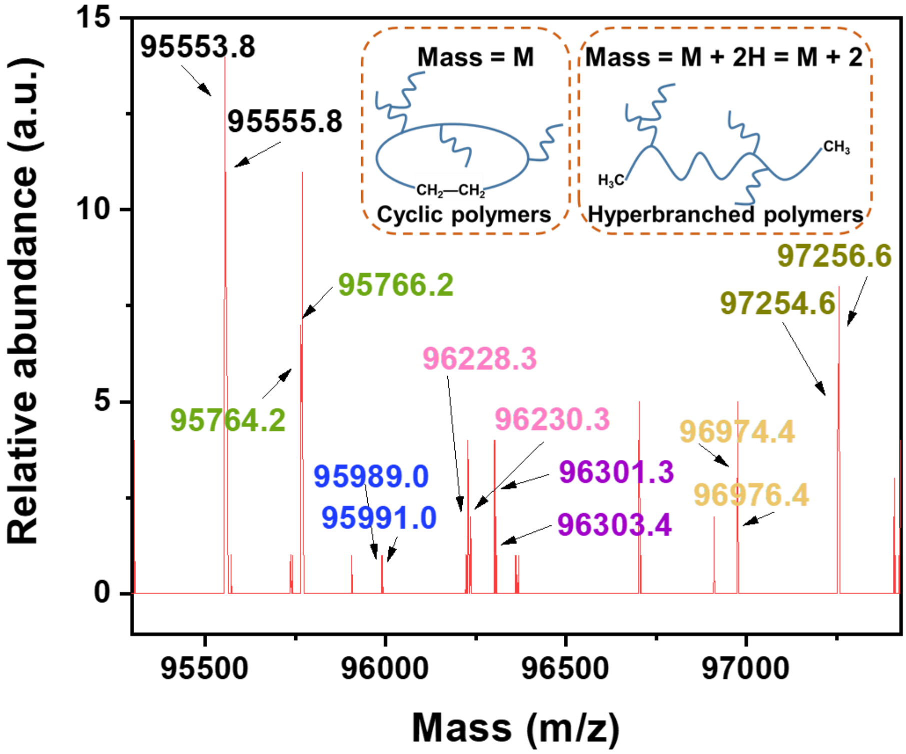

Figure S3. Expansion of MALDI-TOF-MS spectrum for CPDOL.

MALDI-TOF-MS spectra can be used to determine the structure of polymers.[4] According to the mechanism of free radical-initiated polymerization, CPDOL synthesis undergoes chain initiation, chain propagation and chain termination stages.[5] Because the precursor PDOLUDMA has 2 C=C bonds, it is capable of forming hyperbranched polymer structures (**Figure S12**b), and the intermediate of CPDOL with free radicals of $–CH_2·$ is terminated by the abstraction of the corresponding amount of allylic hydrogens from PDOLUDMA monomers. When the last two free radicals in a branched CPDOL intermediate are connected without getting 2 allylic hydrogens, the branched CPDOL intermediate become cyclic CPDOL with $–CH_2–CH_2–$ (Mass = 28 m/z). While when the last two radicals get 2 allylic hydrogens, its chain growth is terminated and it becomes two methyl groups (2 $–CH_3$, Mass = 30 m/z). Thus, in this case, the CPDOL with branched structure has two more hydrogen atoms than the cyclic CPDOL. This results coincide with the M and M+2 results in the MALDI-TOF-MS spectrum(**Figure S3**), indicating that cyclic CPDOL and hyperbranched CPDOL were successfully synthesized.

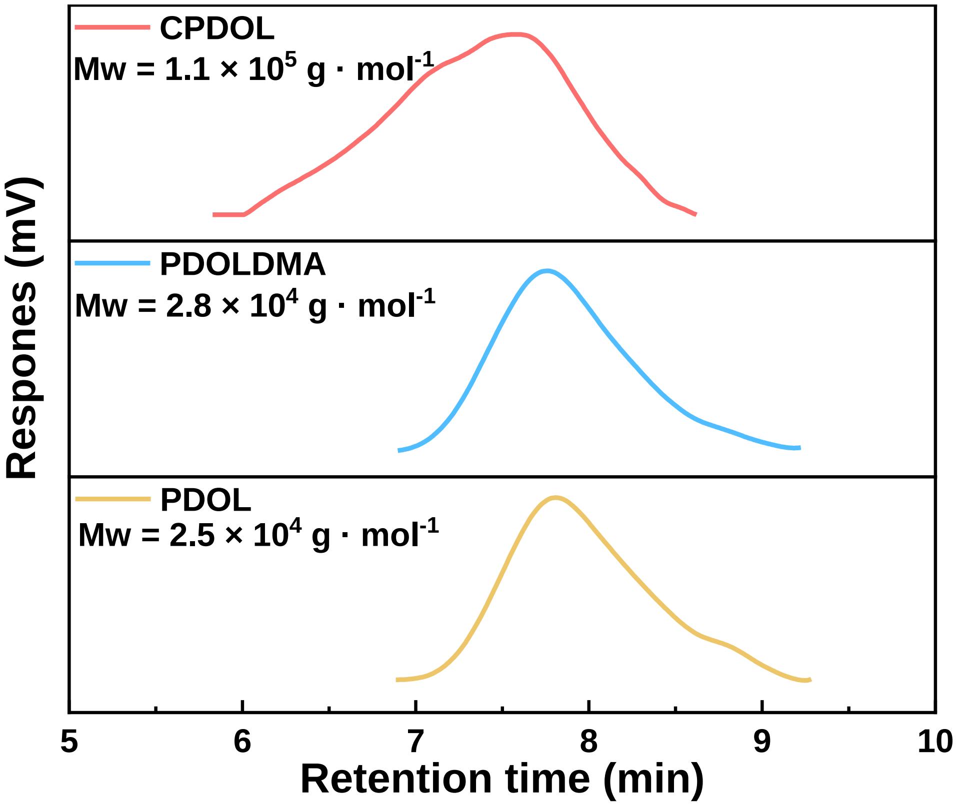

Figure S4. GPC curves of PDOL, PDOLUDMA and CPDOL.

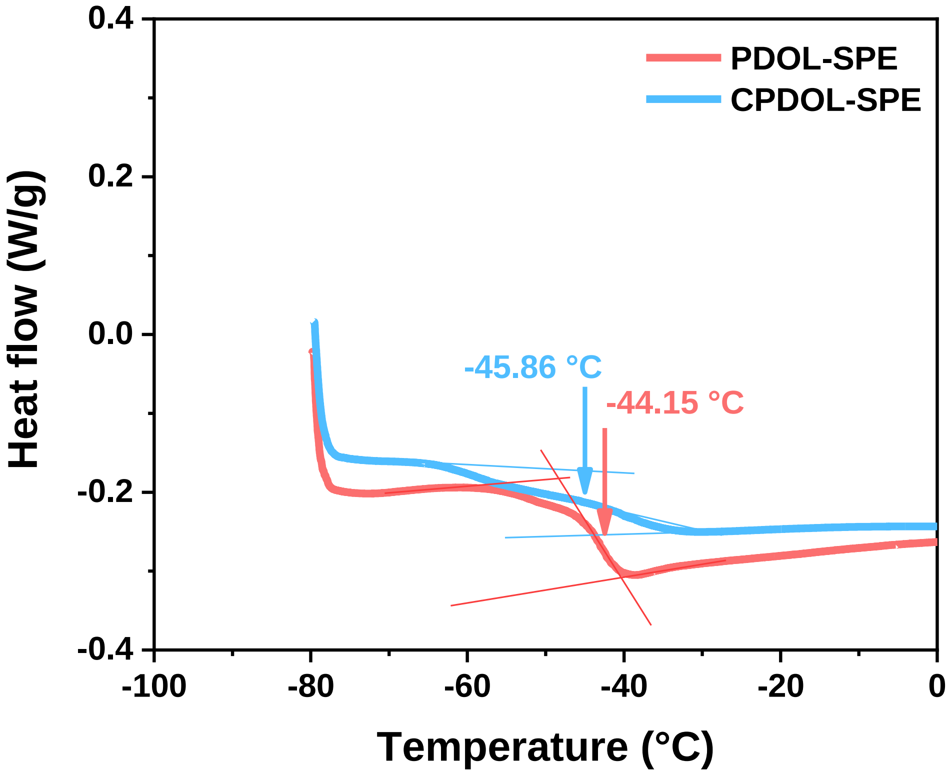

Figure S5. DSC curves of PDOL-SPE and CPDOL-SPE.

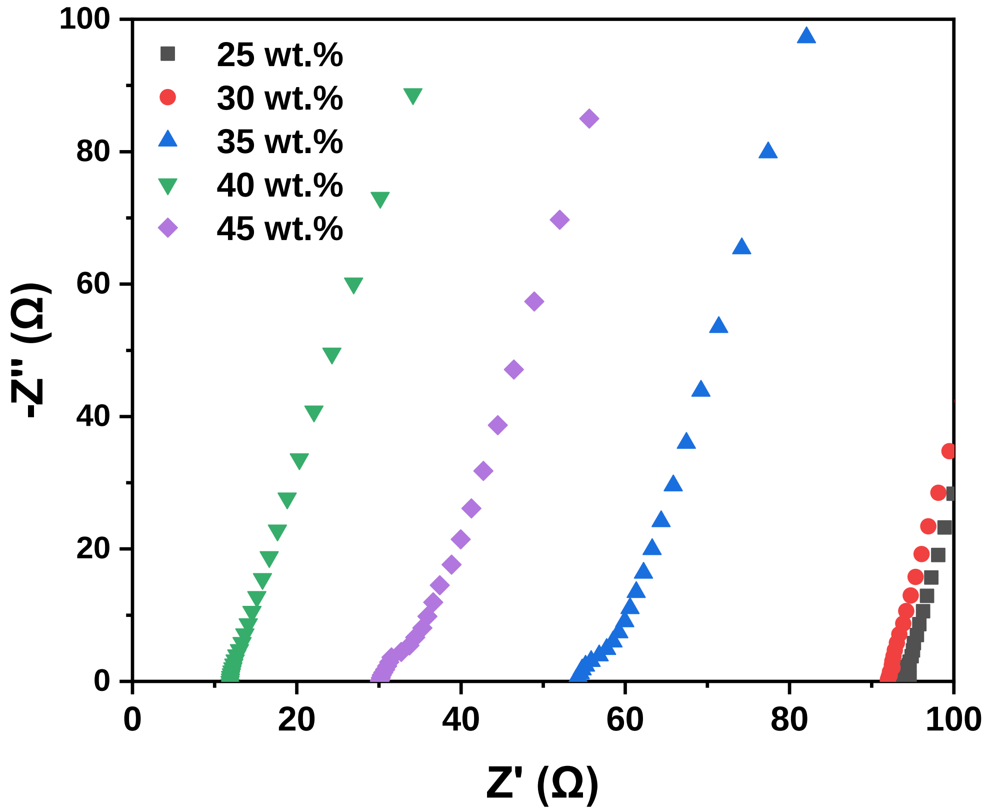

Figure S6. Ionic conductivity at different salt concentrations.

AC impedance results show that CPDOL-SPE exhibites the highest ionic conductivity when the LiTFSI concentration is 40% wt. (**Figure S6**).

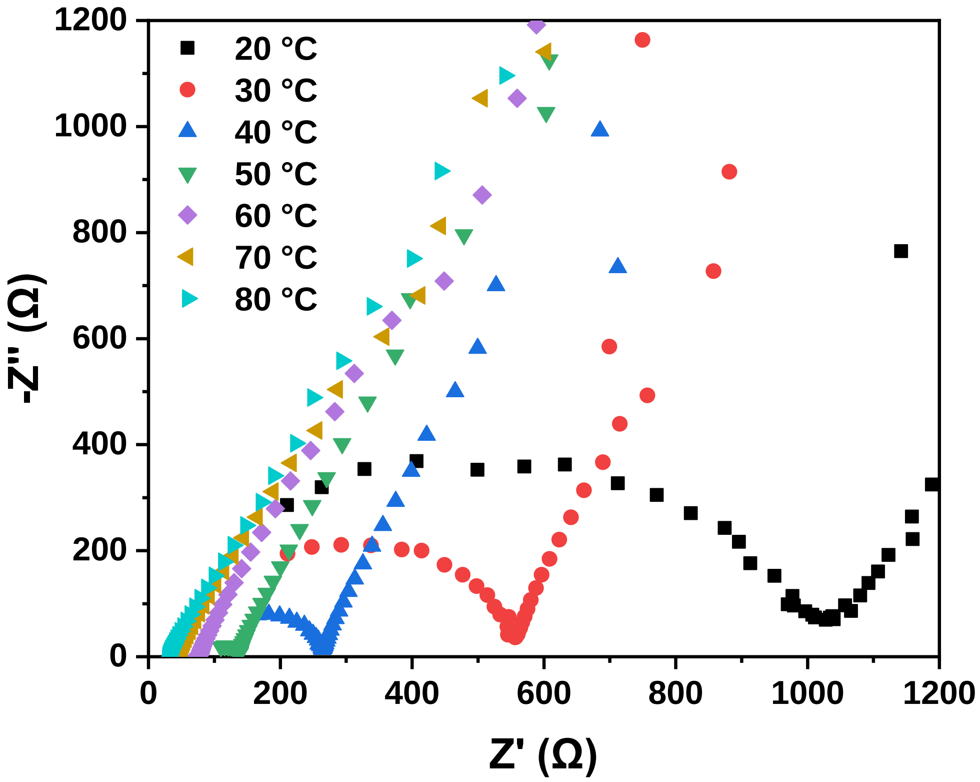

Figure S7. Nyquist plots of CPDOL-SPE in different temperatures.

As shown in **Figure S7**, the primary CPDOL-SPE (deposition thickness = 146 μm) delivers a high ionic conductivity (1.01×10^{-4} S cm^{-1}) at 60 ^{o}C, which proves that the lower Tg can improve ionic conductivity.

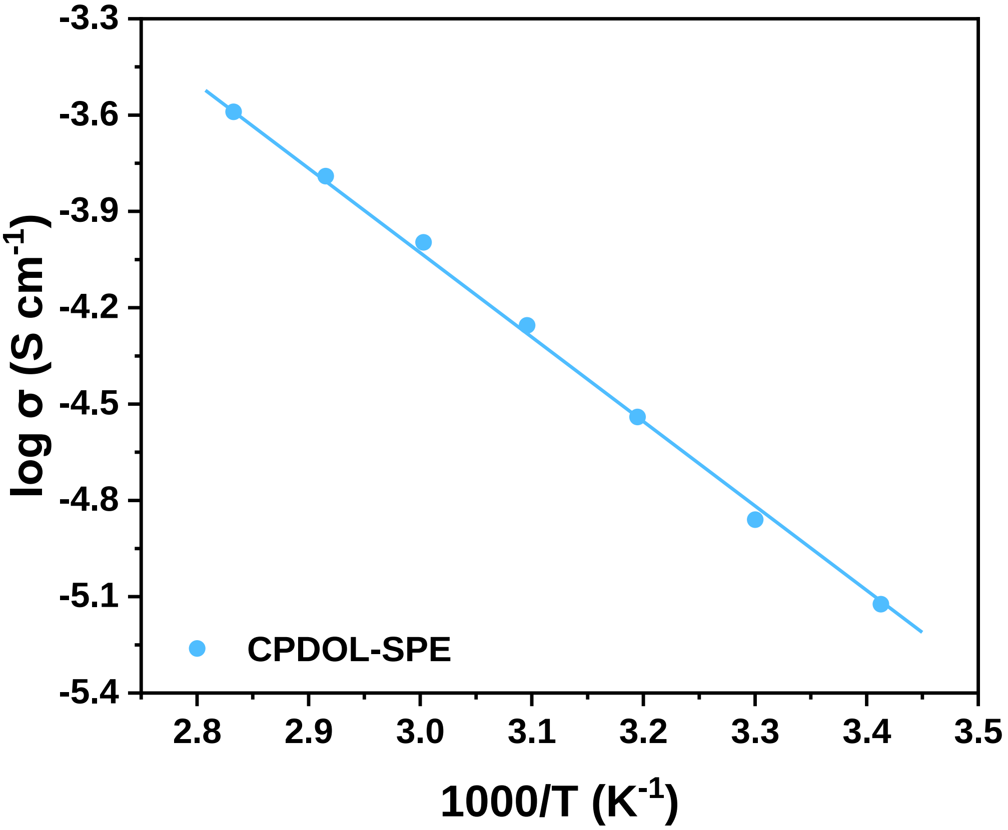

Figure S8. Temperature-dependent curve of ionic conductivities of CPDOL-SPE.

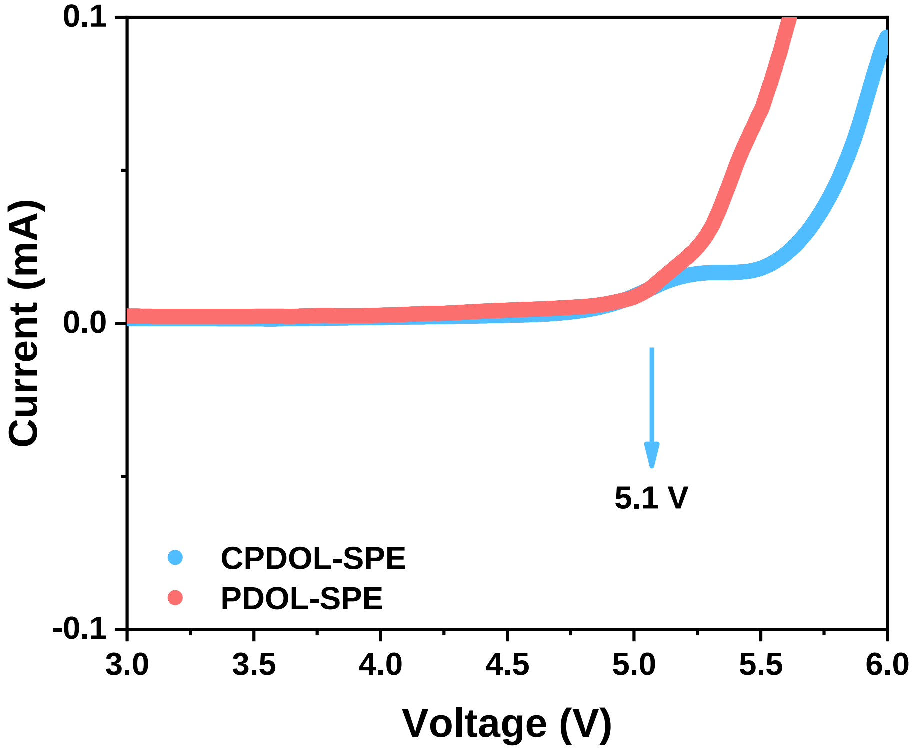

Figure S9. LSV curves of PDOL-SPE and CPDOL-SPE.

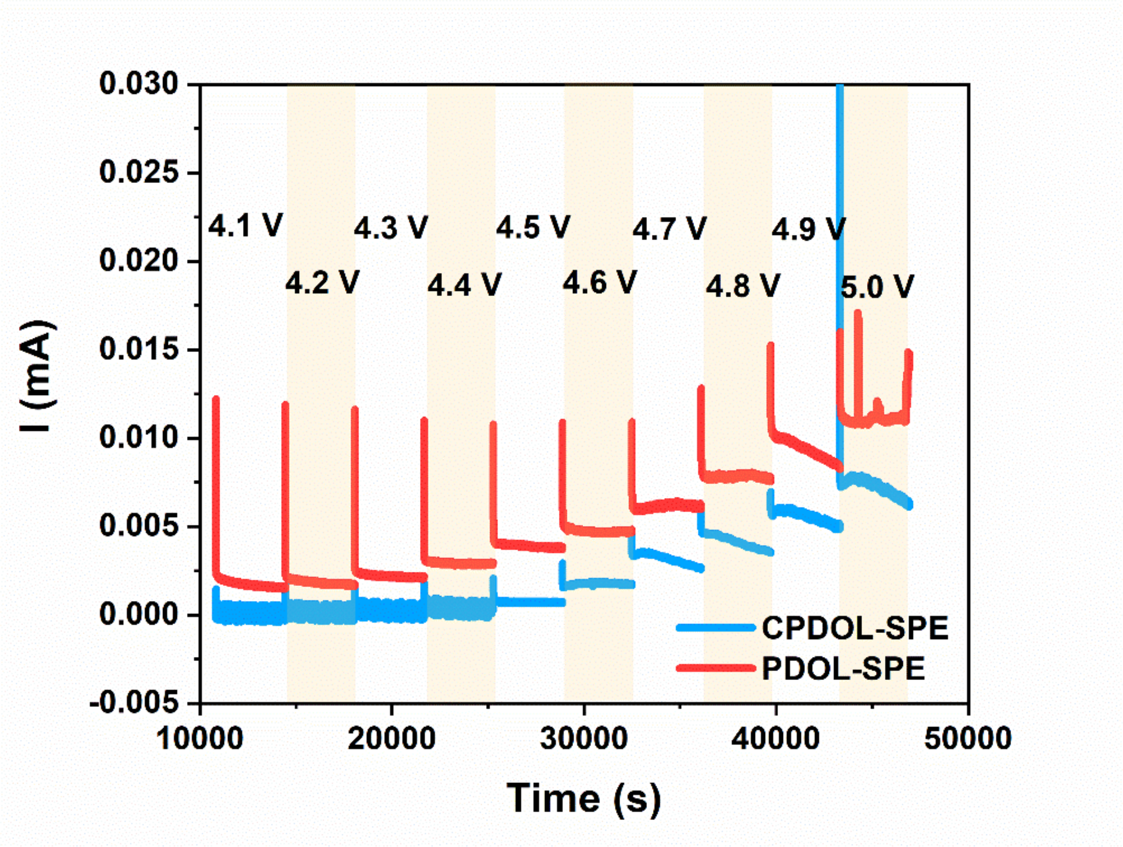

Figure S10. Electrochemical floating curves of the PDOL-SPE and CPDOL-SPE.

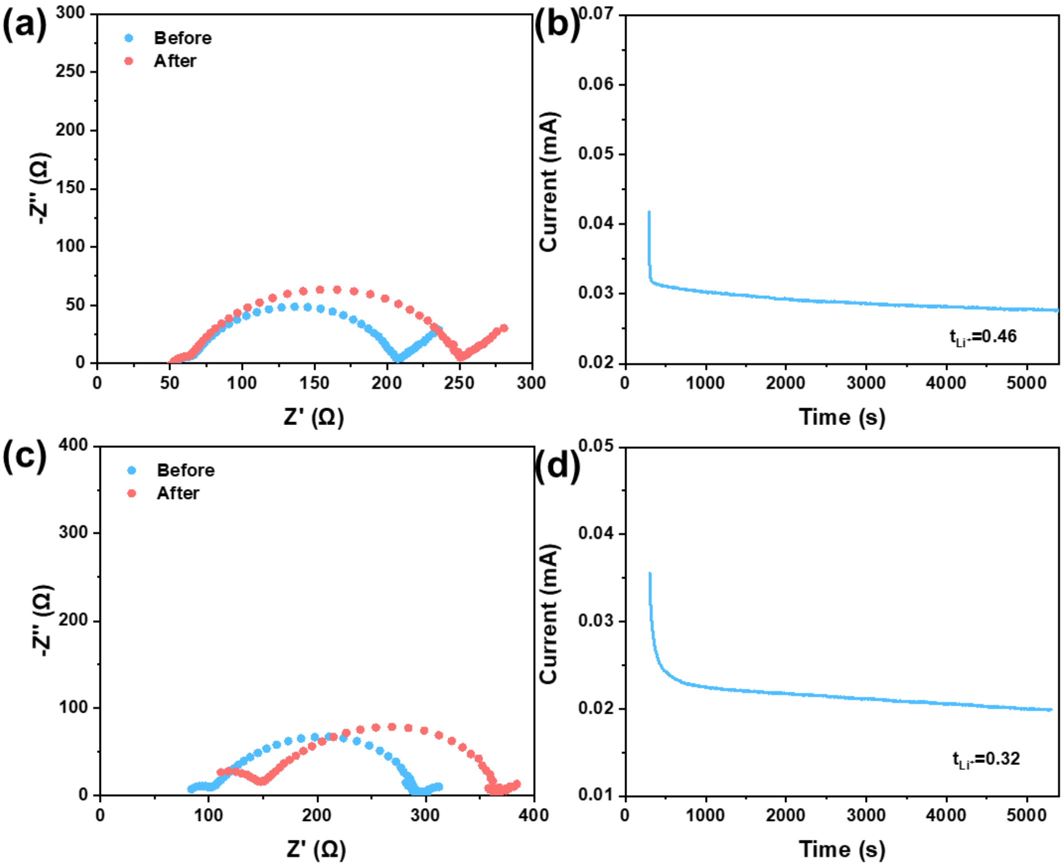

Figure S11. (a) Nyquist profiles of CPDOL-SPE of electrochemical impedance spectroscopy before and after polarization. (b) The corresponding current-time profiles following a DC polarization of 0.01 V for the Li/CPDOL-SPE/Li symmetrical cell at elevated temperature. (c) Nyquist profiles of PDOL-SPE of electrochemical impedance spectroscopy before and after polarization. (d) The corresponding current-time profiles following a DC polarization of 0.01 V for the Li/PDOL-SPE/Li symmetrical cell at elevated temperature.

The time-current curve of the Li/CPDOL-SPE/Li symmetric cell following a direct current (DC) polarization of 0.01 V for 5000 s at 60 °C is presented in **Figure S11**b. As we can see, the initial current is 41.7 μA and then stabilizes at 27.8 μA after polarization, and the corresponding interfacial impedance increases from 166 Ω to 201 Ω (**Figure S11**a). As a result, the CPDOL-SPE presents a t_{Li}^{+} of 0.46, obviously higher than the value (~0.2) of the PEO counterpart. In contrast, the time-current curve of the Li/PDOL-SPE/Li symmetric cell following a direct current (DC) polarization of 0.01 V for 5000 s at 60 °C is presented in **Figure S11**d. The initial current is 35.5 μA and then stabilizes at 19.9 μA after polarization, and the corresponding interfacial impedance increases from 190.1 Ω to 220.8 Ω (**Figure S11**c). The calculated t_{Li}^{+} of PDOL-SPE is 0.32.

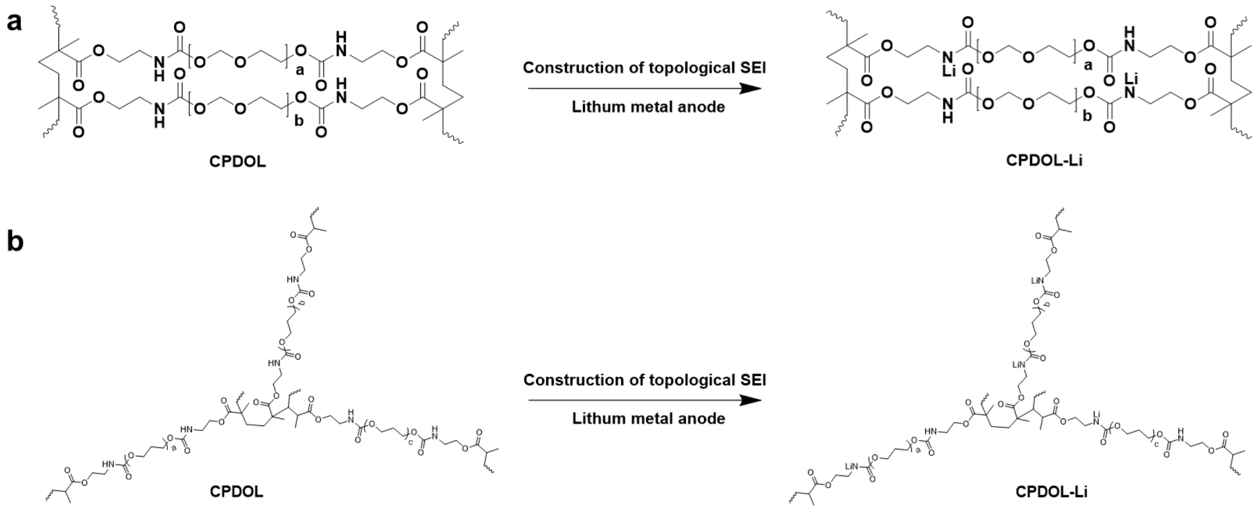

Figure S12. The proposed reaction of in-situ forming two of the topological SEI layers from two of the topological CPDOLs. (a) Cyclic CPDOL. (b) Hyperbranched CPDOL.

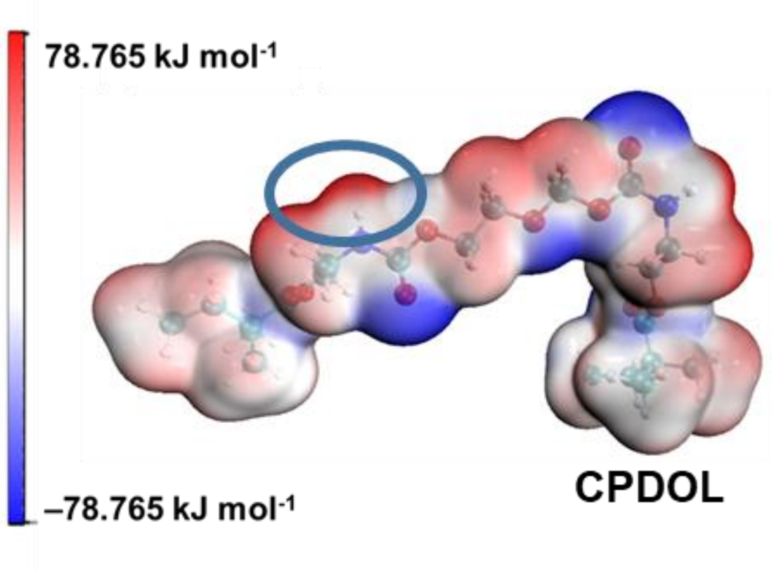

Figure S13. The calculated electrostatic potential map of CPDOL fragment.

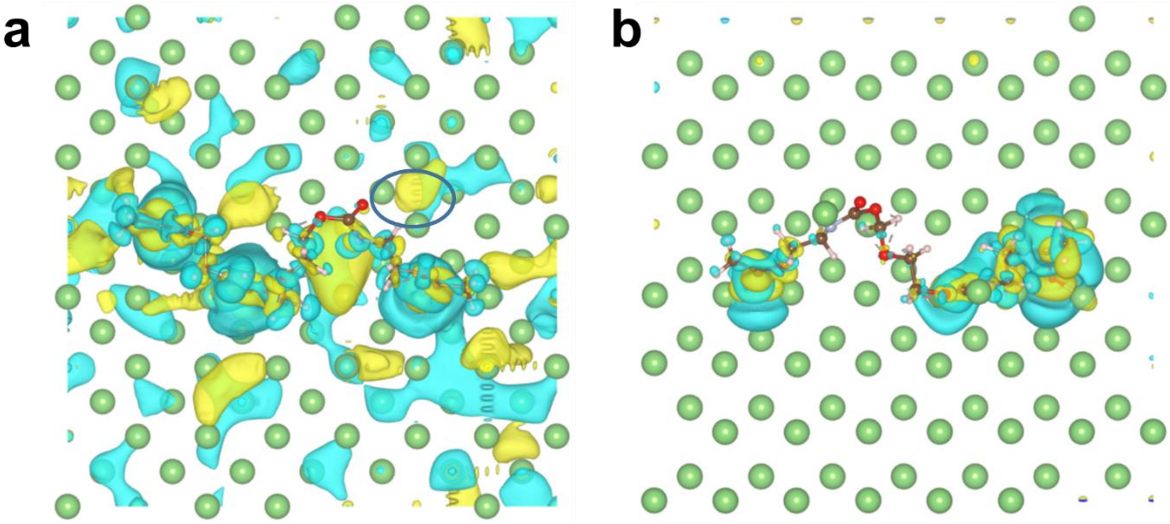

Figure S14. (a) DFT calculation model and differential charge density map of CPDOL. (b) DFT calculation model and differential charge density map of CPDOL-Li.

The blue region is the region where the electron density decreases and the yellow region is the region where the electron density increases. The difference between a and b indicates that a large number of electrons on the lithium metal are transferred to the CPDOL chain segment, causing structural instability, while CPDOL-Li has less electron transfer with lithium and has higher structural stability.

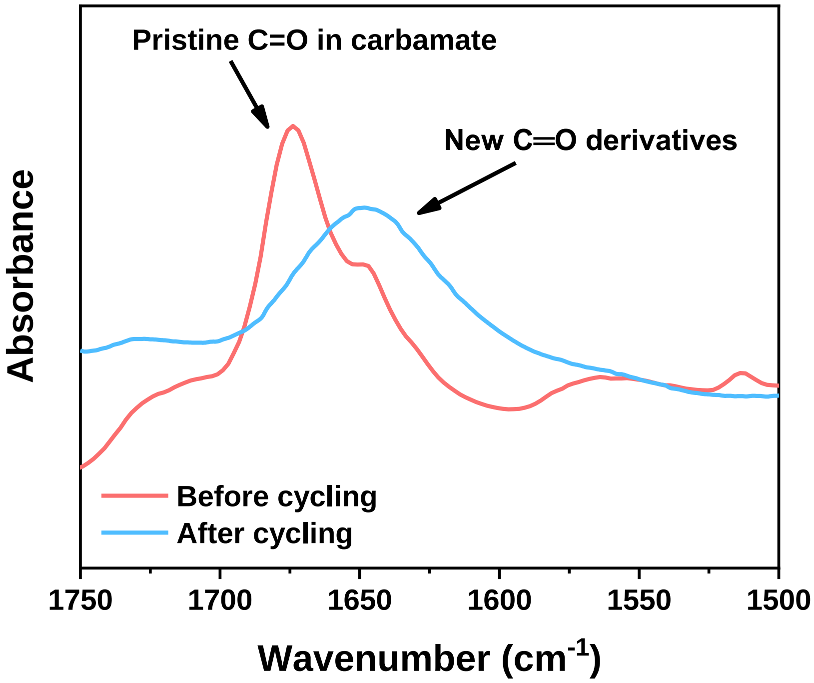

Figure S15. FT-IR spectra of CPDOL-SPE before and after 10 cycles.

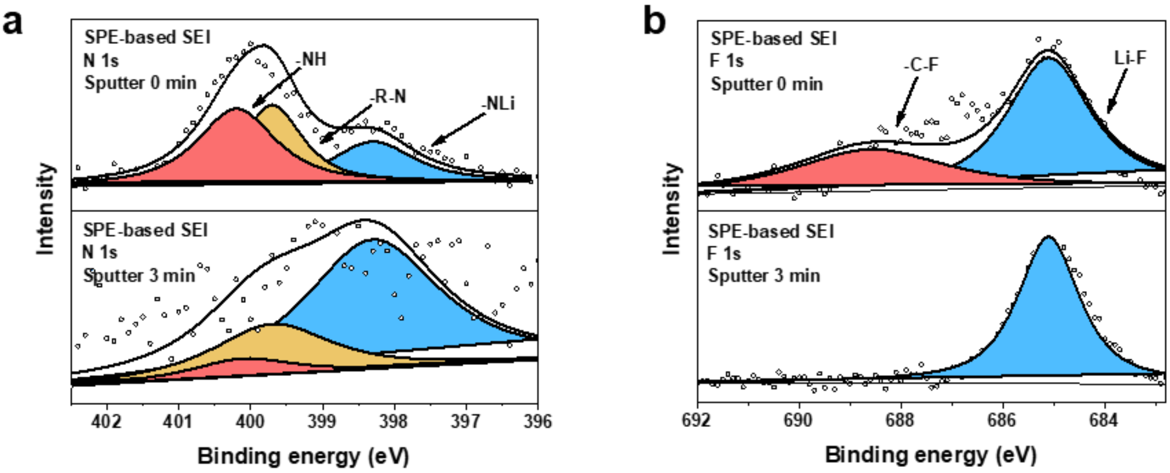

Figure S16. (a) XPS spectra of N 1s on Li metal anode in CPDOL-SPE after different sputtering times. (b) XPS spectra of F 1s on Li metal anode in CPDOL-SPE after different sputtering times.

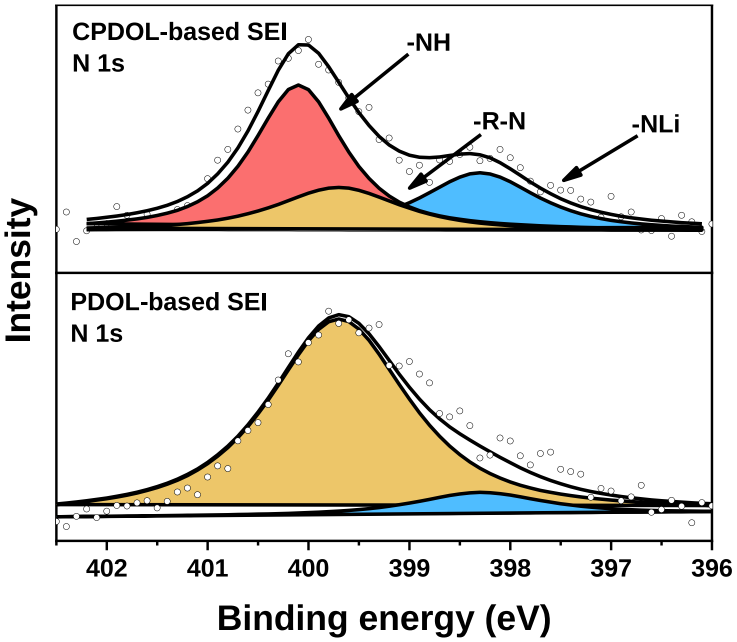

Figure S17. XPS N 1s spectra of the PDOL-based SEI and CPDOL-based SEI after 10 cycles.

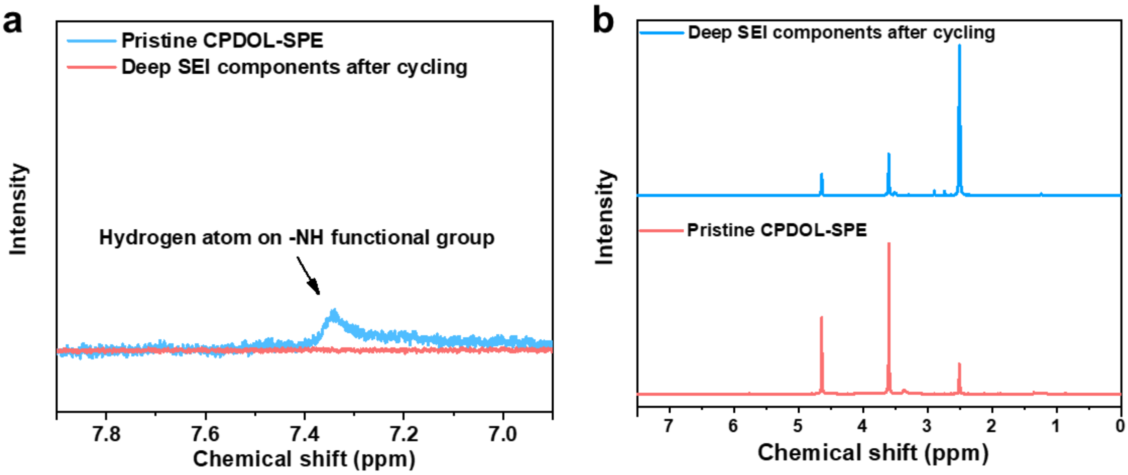

Figure S18. ^{1}H NMR spectra of CPDOL-SPE before cycling and deep SEI component after cycling. (a) Enlarged image. (b) Full image.

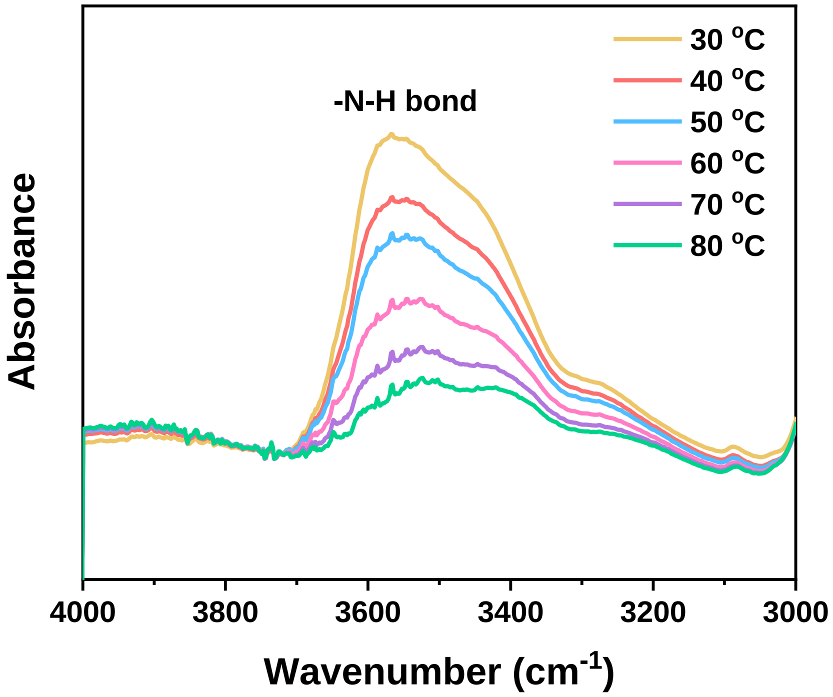

Figure S19. Temperature-dependent FT-IR spectra of CPDOL-SPE.

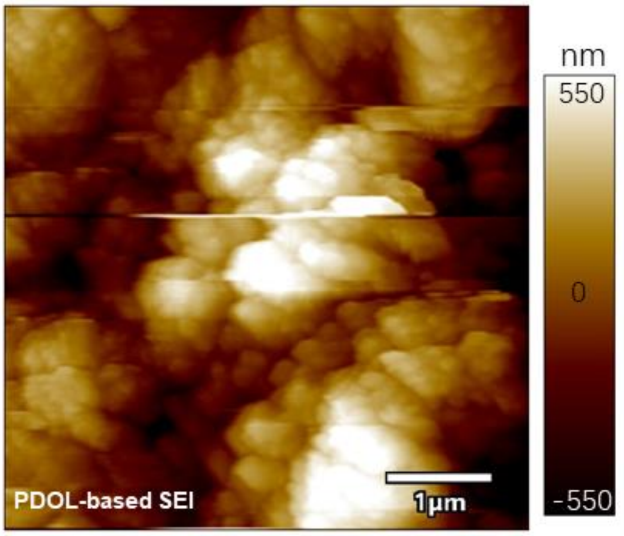

Figure S20. AFM height image of PDOL-based SEI.

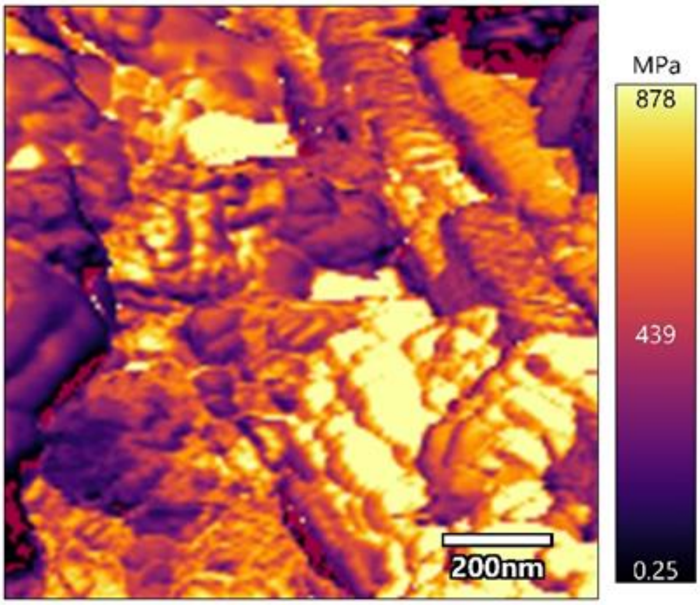

Figure S21. Surface map of Young's modulus of PDOL-based SEI.

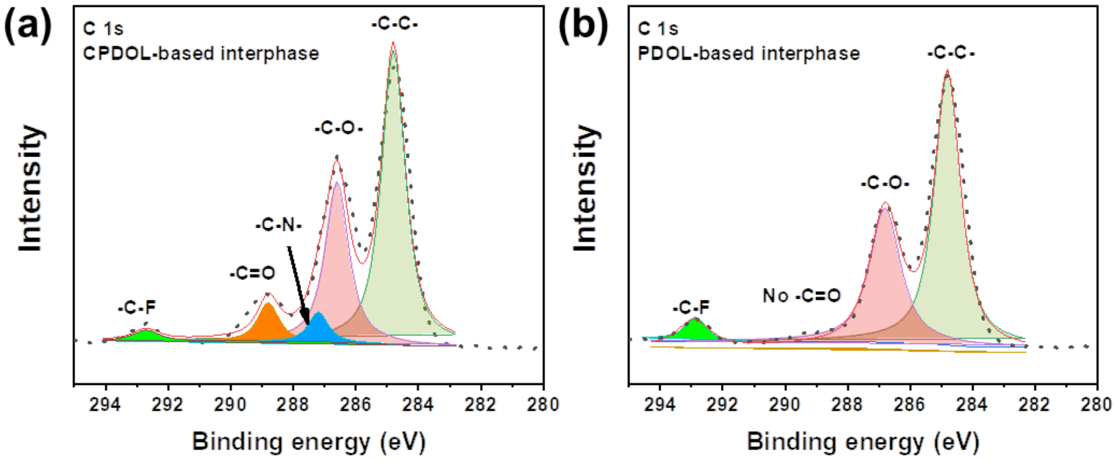

Figure S22. XPS spectra of C 1s of (a) CPDOL-based SEI and (b) PDOL-based SEI after 10 cycles.

Compared with PDOL-based interphase (**Figure S22**b), the CPDOL-based topological interphase (**Figure S22**a) has an abundance of C=O− and −N−.

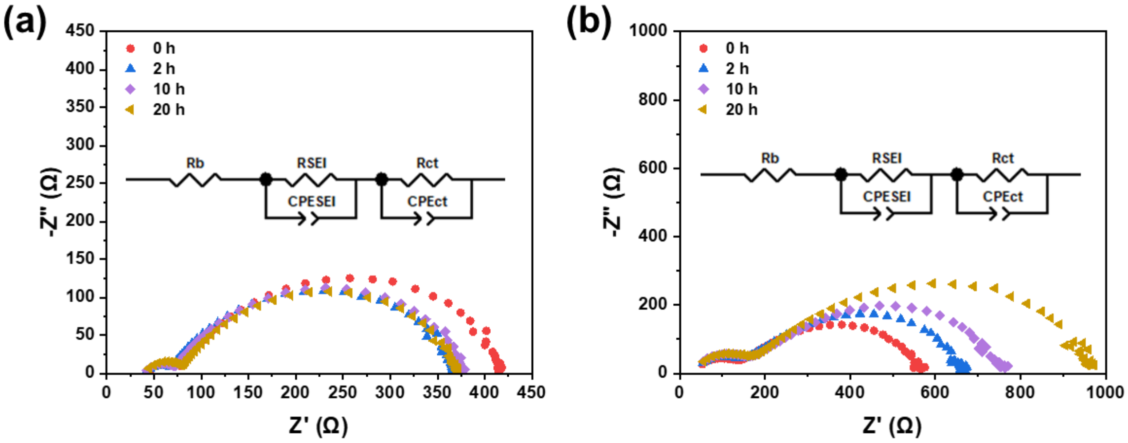

Figure S23. (a) Nyquist plot of the impedance of Li/CPDOL-SPE/Li at different cycles. (b) Nyquist plot of the impedance of Li/PDOL-SPE/Li at different cycles.

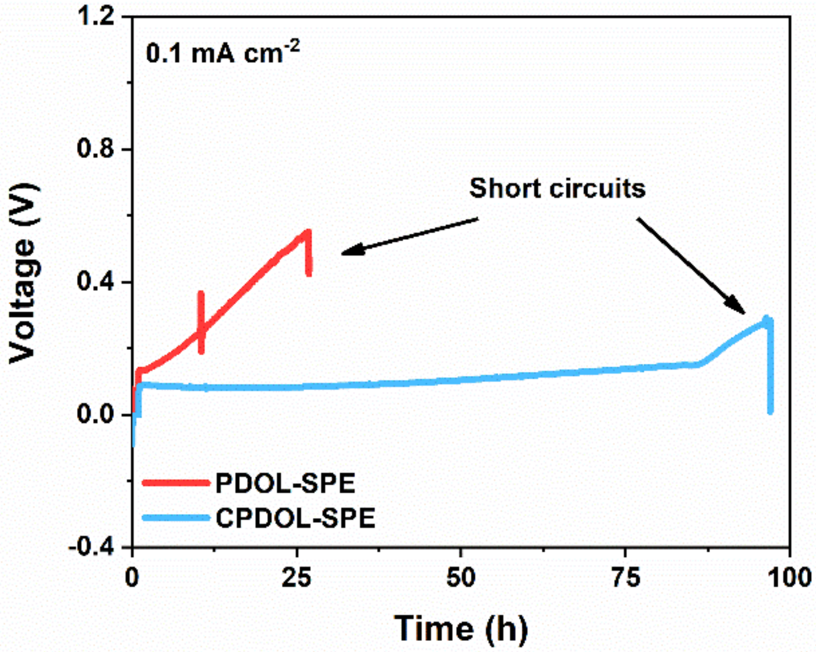

Figure S24. Sand's times of PDOL-SPE and CPDOL-SPE.

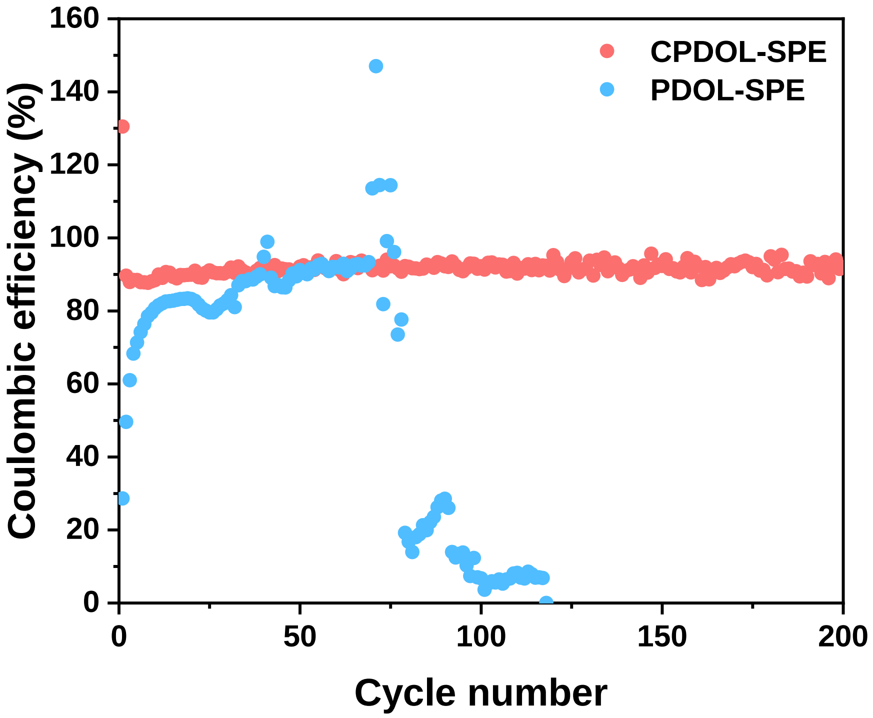

Figure S25. Coulombic efficiencies of Li plating/stripping in Cu/Li cells using CPDOL-SPE and PDOL-SPE at 0.136 mA cm^{-2} and 0.136 mAh cm^{-2}.

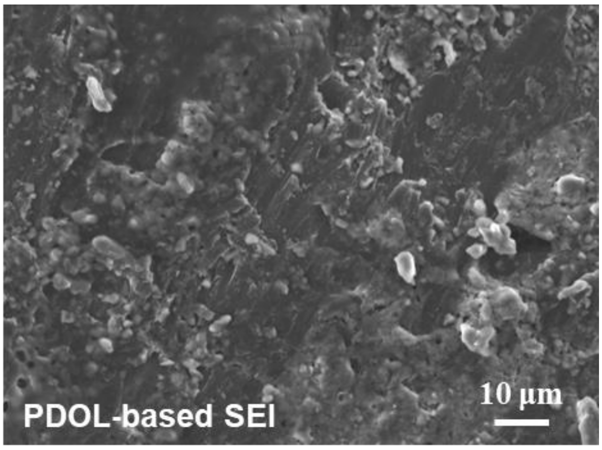

Figure S26. Top-view SEM image of PDOL-based SEI after 50 cycles.

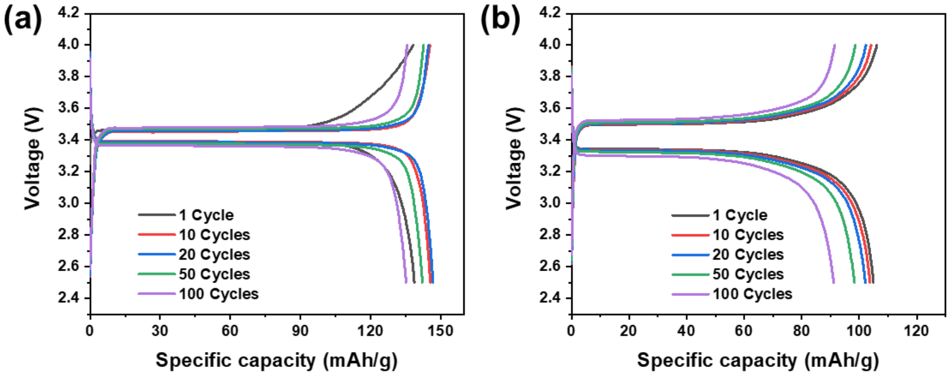

Figure S27. (a) Charge/discharge profiles of the PDOL-SPE-based LFP/Li cell at 0.25 C and different cycles. (b) Charge/discharge profiles of the PDOL-SPE-based LFP/Li cell at 0.5 C and different cycles.

Figure S28. LiFePO_4/CPDOL-SPE/Li pouch battery after cutting.

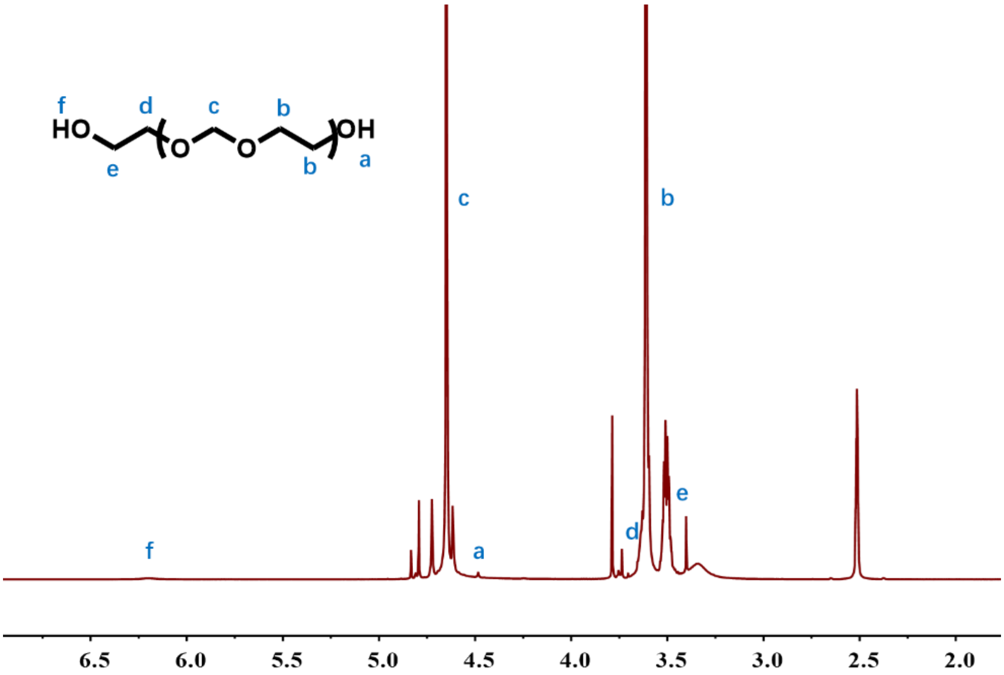

Figure S29. ^{1}H NMR (400 MHz, DMSO-d_6) of hydroxyl-terminated PDOL.

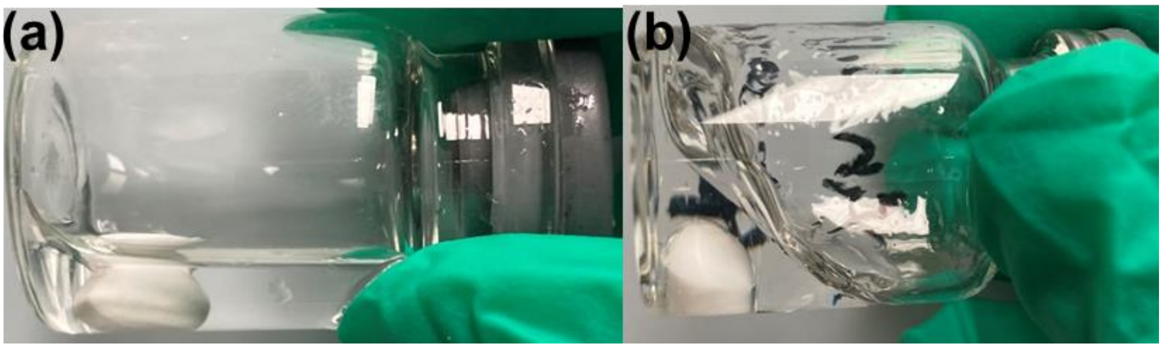

Figure S30. The status of PDOLUDMA dissolved in DMF before (a) and after (b) polymerization.

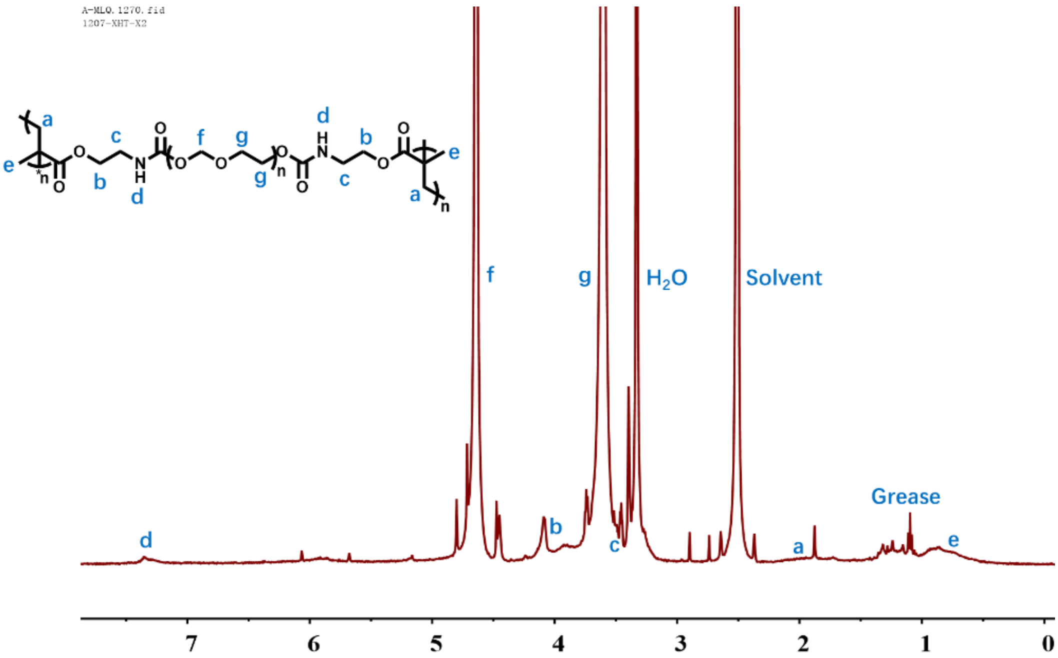

Figure S31. ^{1}H NMR (400 MHz, DMSO-d$_6$) of CPDOL.

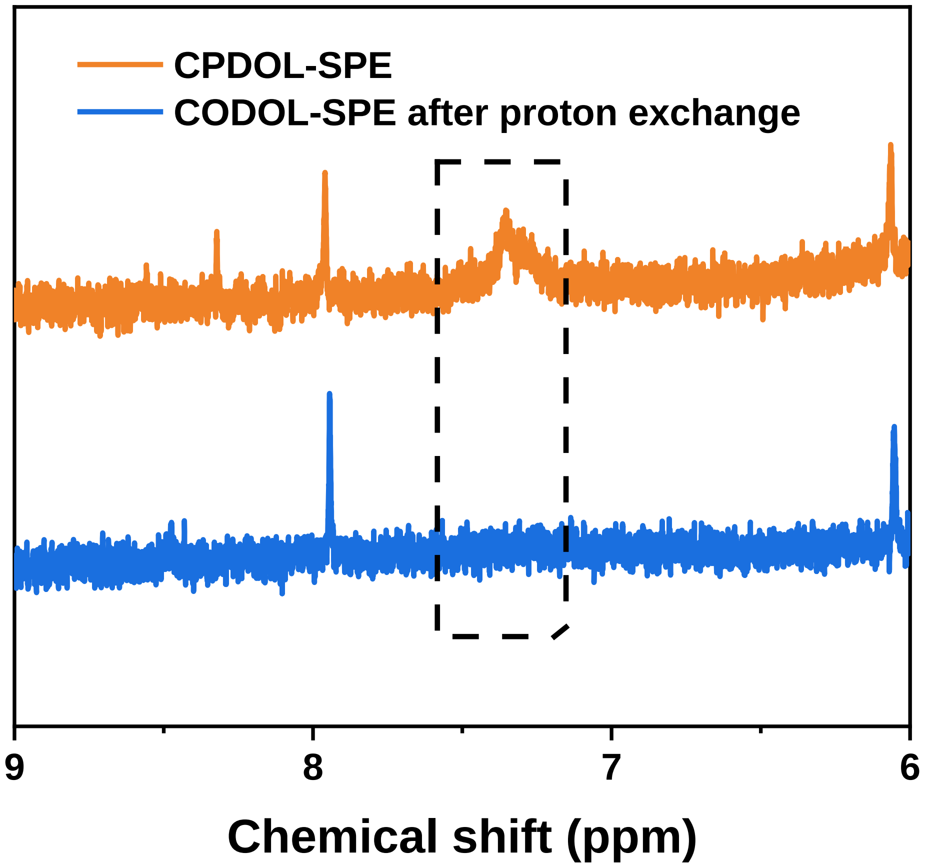

Figure S32. ^{1}H NMR of CPDOL-SPE before and after proton exchange.

Table S1. HOMO and LUMO levels of PDOL and CPDOL.

	HOMO (eV)	LUMO (eV)
PDOL	-7.02	0.834
CPDOL	-7.33	0.109

Table S2. Fitting results of R_{SEI} of Li/Li cells assembled with CPDOL-SPE and PDOL-SPE at different temperatures after 10 cycles.

Temperature (°C)	PDOL-SPE (Ω)	CPDOL-SPE (Ω)
20	6751.3	3927.2
30	2121.8	1502.8
40	748.61	595.53
50	296.63	237.23
60	110.7	90.304

Table S3. Elements content of SEI surface by XPS quantitative analysis.

	RSF	Atomic con. [%]	Error [%]	Mass con. [%]	Error [%]
N 1s	0.477	1.506161	0.256318	1.733999	0.292358
F 1s	1	1.085116	0.187623	1.694472	0.289212
Li 1s	0.025	13.75837	2.149804	7.85035	1.310735
C 1s	0.278	64.92533	1.67421	64.09676	1.046294
O 1s	0.78	18.72502	0.585651	24.62442	0.565558

Table S4. Typical performance and stable time at 60 °C of solid-polymer-electrolyte-based Li/Li cells in recent years.

Type	Current density (mA cm^{-2})	Overpotential at stable state (mV vs. Li/Li^{+})	Stable time (h)	Year	Reference
PEO with LAGP	0.1	170	>400	2019	[6]
MIP-SPE	0.2	~60	100	2021	[7]
PEO/MnO_2/LiTFSI	0.1	70	800	2020	[8]
PVA/UPy/PEG/$LiClO_4$	0.05	~100	500	2019	[9]
IMFPIL-LiTFSI	0.1	80	250	2019	[10]
CHPEs-Li	0.1	170	1400	2019	[11]
PEO-LPS	0.05	25	1000	2022	[12]
CN-PEO	0.1	48	1000	2022	[13]
PEO-MOF-2	0.1	~50	350	2022	[14]
PSi–S–CN-10	0.1	10	1000	2021	[15]
CPDOL-SPE	0.1	62	3000		This work

Table S5. Fitting results of R_{bulk}, R_{SEI} and R_{ct} of Li/Li cells assembled with CPDOL-SPE and PDOL-SPE at different cycles.

CPDOL-SPE				PDOL-SPE			
Time (h)	R_b (Ω)	R_{SEI} (Ω)	R_{ct} (Ω)	Time (h)	R_b (Ω)	R_{SEI} (Ω)	R_{ct} (Ω)
0	43.696	42.043	337.04	0	31.49	142.34	444.07
2	40.356	36.589	299.73	2	27.808	168.87	503.29
10	39.763	39.768	304.56	10	31.017	167.77	609.01
20	40.649	44.48	292.12	20	23.293	196.84	731.72

Table S6. Typical performance of polymer-electrolyte-based $LiFePO_4$/Li cells in recent years.

Type	Rate (C)	Capacity retention	Number of cycles	Loading mass (mg cm^{-2})	Temperature (^oC)	Year	Reference
IMFPIL-LiTFSI	0.2	73%	150	1.5	60	2019	[10]
MICs	1/3	83%	500	3	60	2021	[16]
CHPEs-Li	0.2	90%	200	Low	60	2019	[11]
PAN-PEO	0.5	70%	500	3	60	2022	[17]
HEMI-ASPE-Li	0.41	96%	300	1-2	70	2022	[18]
CPDOL-SPE	0.5	95.1%	500	0.8-1.8	60		This work

References

[1] a) G. Kresse, J. Furthmüller, *Computational Materials Science* **1996**, 6, 15; b) G. Kresse, J. Furthmüller, *Physical Review B* **1996**, 54, 11169.

[2] J. P. Perdew, K. Burke, M. Ernzerhof, *Physical Review Letters* **1996**, 77, 3865.

[3] a) S. Grimme, J. Antony, S. Ehrlich, H. Krieg, *The Journal of Chemical Physics* **2010**, 132, 154104; b) S. Grimme, S. Ehrlich, L. Goerigk, *Journal of Computational Chemistry* **2011**, 32, 1456.

[4] D. Hua, X. Ge, J. Tang, X. Zhu, R. Bai, *European Polymer Journal* **2007**, 43, 847.

[5] A. Matsumoto, T. Kumagai, H. Aota, H. Kawasaki, R. Arakawa, *Polymer Journal* **2009**, 41, 26.

[6] X. Wang, H. Zhai, B. Qie, Q. Cheng, A. Li, J. Borovilas, B. Xu, C. Shi, T. Jin, X. Liao, Y. Li, X. He, S. Du, Y. Fu, M. Dontigny, K. Zaghib, Y. Yang, *Nano Energy* **2019**, 60, 205.

[7] J. Seo, G.-H. Lee, J. Hur, M.-C. Sung, J.-H. Seo, D.-W. Kim, *Advanced Energy Materials* **2021**, 11, 2102583.

[8] Y. Li, Z. Sun, D. Liu, Y. Gao, Y. Wang, H. Bu, M. Li, Y. Zhang, G. Gao, S. Ding, *Journal of Materials Chemistry A* **2020**, 8, 2021.

[9] Y. H. Jo, B. Zhou, K. Jiang, S. Li, C. Zuo, H. Gan, D. He, X. Zhou, Z. Xue, *Polymer Chemistry* **2019**, 10, 6561.

[10] Y. Zhou, Y. Yang, N. Zhou, R. Li, Y. Zhou, W. Yan, *Electrochimica Acta* **2019**, 324, 134827.

[11] C. Zuo, M. Yang, Z. Wang, K. Jiang, S. Li, W. Luo, D. He, C. Liu, X. Xie, Z. Xue, *Journal of Materials Chemistry A* **2019**, 7, 18871.

[12] P. Mirmira, C. Fuschi, W. Gillett, P. Ma, J. Zheng, Z. D. Hood, C. V. Amanchukwu, *ACS Applied Energy Materials* **2022**, 5, 8900.

[13] H. Liang, S. Wang, Q. Ye, C. Zeng, Z. Tong, Y. Ma, H. Li, *Chemical Communications* **2022**, 58, 10821.

[14] G. Lu, H. Wei, C. Shen, F. Zhou, M. Zhang, Y. Chen, H. Jin, J. Li, G. Chen, J. Wang, S. Wang, *ACS Applied Materials & Interfaces* **2022**, 14, 45476.

[15] C. Fu, M. Iacob, Y. Sheima, C. Battaglia, L. Duchêne, L. Seidl, D. M. Opris, A. Remhof, *Journal of Materials Chemistry A* **2021**, 9, 11794.

[16] D. Yu, X. Pan, J. E. Bostwick, C. J. Zanelotti, L. Mu, R. H. Colby, F. Lin, L. A. Madsen, *Advanced Energy Materials* **2021**, 11, 2003559.

[17] Y. Ma, J. Wan, Y. Yang, Y. Ye, X. Xiao, D. T. Boyle, W. Burke, Z. Huang, H. Chen, Y. Cui, *Advanced Energy Materials* **2022**, 12, 2103720.

[18] Y. Su, X. Rong, H. Li, X. Huang, L. Chen, B. Liu, Y. S. Hu, *Advanced Materials* **2022**, 2209402.